Journal of Achievements in Materials and Manufacturing Engineering
VOLUME 46
ISSUE 2
June
2011

Thermal and structure analysis of the MA MgAl6Zn3 magnesium alloy

L.A. Dobrzański*, M. Król
Division of Materials Processing Technology, Management and Computer Techniques in Materials Science, Institute of Engineering Materials and Biomaterials, Silesian University of Technology, ul. Konarskiego 18a, 44-100 Gliwice, Poland
* Corresponding author: E-mail address: leszek.dobrzanski@polsl.pl

Received 20.04.2011; published in revised form 01.06.2011

Manufacturing and processing

ABSTRACT

Purpose: This work presents effect of cooling rate structural properties and thermal characteristic results of MA MgAl6Zn3 cast alloy.
Design/methodology/approach: The experiments were performed using the novel Universal Metallurgical Simulator and Analyzer Platform. Material used in this experiment is experimental magnesium alloy made as-cast.
Findings: The research show that the thermal analysis carried out on UMSA Technology Platform is an efficient tool for collect and calculate thermal parameters. The formation temperatures of various thermal parameters and grain size are shifting with an increasing cooling rate.
Research limitations/implications: This paper presents results for one alloy - MA MgAl6Zn3 only, cooled with three different solidifications rate i.e. 0.6, 1.2 and 2.4ºC/s, for assessment for the liquidus, solidus and others temperatures and its influence on the structure.
Practical implications: The parameters described can be applied in metal casting industry for selecting magnesium ingot preheating temperature for semi solid processing to achieve requirements properties.
Originality/value: The paper contributes to better understanding and recognition an influence of different solidification condition on non-equilibrium thermal parameters of magnesium alloys.
Keywords: Thermal treatment; Magnesium alloys; Mechanical properties

Reference to this paper should be given in the following way:
L.A. Dobrzański, M. Król, Thermal and structure analysis of the MA MgAl6Zn3 magnesium alloy, Journal of Achievements in Materials and Manufacturing Engineering 46/2 (2011) 189-195.

1. Introduction

Mg-Al alloys have a very wide application because of their excellent properties, low manufacture cost, easy melting technique and no expensive elements content [1]. One of this kind alloys, AZ63 magnesium alloy, is a widely applied magnesium sacrificial anode which is used extensively in underground and freshwater at present. However, compared with that aboard, home sacrificial anode has some demerits: low current efficiency and weak protection function, so investigating the high driving-potential and high efficiency sacrificial anodes is a very significant thing at present. Different alloying elements additions would different effects on the microstructure and properties of magnesium alloys, so many alloying elements additions have been magnesium in an attempt to improve microstructure and mechanical properties [2-5].

Maximal solubility of aluminum in magnesium is 12.6 mass % Al at the eutectic temperature of 437°C. Eutectic point of the Mg-Al alloy is determined at 32 mass % Al. Due to the hardening by the precipitation of the intermetallic compound of $Mg_{17}Al_{12}$ under the solidus line the aluminum addition increases the tensile stress and hardness. Aluminum is the most used alloying element at the

magnesium alloys, with its content between 2 and 10 mass %. Such alloys have good mechanical properties and excellent corrosion resistance. By the increased aluminum content the castability is improved [6-8].

Negative characteristics of the high aluminum content in the Mg-Al alloy is the formation of the $Mg_{17}Al_{12}$ intermetallic phase, which is precipitating between the αMg dendrite grains and it decreases the tensile stress. It leads to the limited ductility, which is also the characteristic of the alloys with zinc. To improve the workability the aluminum fraction is decreased, the addition of zinc is completely abandoned, what should be replaced by the manganese [9-14].

2. Experimental procedure

2.1. Material

The experiments have been carried out on MA MgAl6Zn3 magnesium alloys in as-cast. The chemical compositions of the investigated materials are given in Table 1.

Table 1.
Average chemical composition (wt%) of the MA MgAl6Zn3 alloy

Al	Zn	Mn	Cu	Ni	Fe
5.7	2.5	0.22	0.004	0.0015	0.0025

2.2. Test sample

The experiments were performed using a pre-machined cylindrical test sample with a diameter of ϕ=18 mm and length of l=20 mm taken from the ingot (Fig. 1). In order to assure high repeatability and reproducibility of the thermal data, the test sample mass was 9.2 g within a very closely controlled range of ±0.1 g. Each sample had a predrilled hole to accommodate a supersensitive K type thermocouple (with extra low thermal time constants) positioned at the center of the test sample to collect the thermal data and control the processing temperatures.

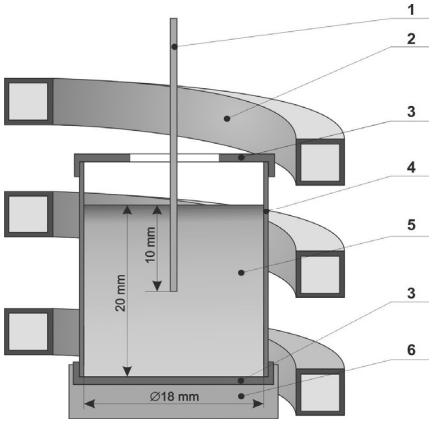

Fig. 1. Schematic of the UMSA Thermal Analysis Platform experimental set-up: 1 - low thermal mass thermocouple, 2 - heating and cooling coil, 3 - thermal insulation, 4 - steel foil, 5 - test sample, 6 - ceramic base

2.3. Thermal analysis

The thermal analysis during melting and solidification cycles was carried out using the Universal Metallurgical Simulator and Analyzer (UMSA) (Fig. 2) [15]. The melting and solidification experiments for the magnesium alloy were carried out using Argon as cover gas. The data for Thermal Analysis (TA) was collected using a high-speed National Instruments data acquisition system linked to a personal computer. Each TA trial was repeated three times to stabilize a process.

The TA signal in the form of heating and cooling curves was recorded during the melting and solidification cycles. The temperature vs. time and first derivative vs. temperature as well as fraction solid vs. temperature were calculated and plotted. The cooling rates for these experiments were determined using the following formula:

$$CR = \frac{T_{liq} - T_{sol}}{t_{sol} - t_{liq}} [\frac{^{\circ}C}{s}] \tag{1}$$

where T_{liq} and T_{sol} are the liquidus and solidus temperatures (°C), respectively, and t_{liq} and t_{sol} the times from the cooling curve that correspond to liquidus and solidus temperatures, respectively.

The procedure comprised of the following steps. First, the test sample was heated to 700±2°C and isothermally kept at this temperature for a period of 90 s in order to stabilize the melt conditions. Next, the test sample was solidified at cooling rate of approximately 0.6°C/s, that was equivalent to the solidification process under natural cooling conditions. To achieve an intentional cooling rate:

- 0.6°C/s sample was cooled without forces air
- 1.2°C/s sample was cooled in airflow 30 l/min,
- 2.4°C/s sample was cooled in airflow 125 l/min.

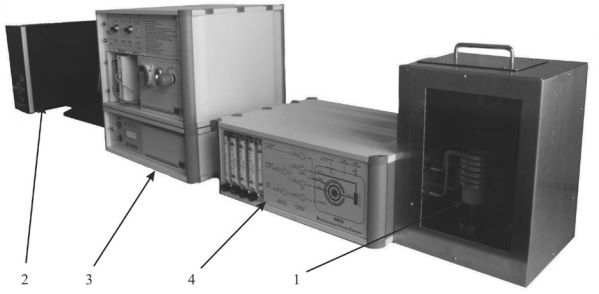

Fig. 2. UMSA apparatus - (1) sample chamber, (2) supervisory computer, (3) temperature control, (4) gas flow control

The magnesium nucleation temperature T_N, T_{Dmin}, T_{DKP}, T_G, and solidus temperatures T_{sol}, where calculated using the first derivative of the cooling curve. The α-Mg Dendrite Nucleation Temperature, ($T^{\alpha DEN}_{NUC}$) represents the point at which primary stable dendrites start to solidify from the melt. This event is

manifested by the change in the slope of the cooling curve and determined by the first derivative inflection point. The liquidus temperature signifies the beginning of the fraction solid that, at this point, is equal to zero. The α-Mg Dendrite Minimum (Undercooling) Temperature, ($T^{\alpha DEN}_{MIN}$) represents a state where the nucleated dendrites have grown to such an extent that the liberated latent heat of fusion balances the heat extracted from the test sample. After passing this point, the melt temperature increases to a steady state growth temperature ($T^{\alpha DEN}_{G}$). $T^{\alpha DEN}_{NUC}$ as the local minimum is determined by the point at which the first derivative intersects the zero line (dT/dt=0). The time period required for heating up of the test sample to the $T^{\alpha DEN}_{G}$ is called recalescence. At the start of solidification of a melt, small equiaxed crystals are developing, separate from one another. The viscosity of the melt and hence torque is very small. As the dendrites grow in size and start to impinge upon one another, a continuous solid network builds up throughout the sample volume. There is a sudden increase in the torque force needed to shear the solid network. This point is called "coherency point". The α-Mg Dendrite Growth Temperature, ($T^{\alpha DEN}_{G}$) represents the local maximum temperature of this reaction (and is also called the "steady state growth temperature). The $T^{\alpha DEN}_{G}$ corresponds to the second zero point on the first derivative curve (dT/dt=0) following the start of nucleation (dT/dt=0). If the first derivative curve in this region does not intersect the zero line, $T^{\alpha DEN}_{MIN}$ the $T^{\alpha DEN}_{G}$ temperatures are identical and correspond to the maximum point on the first derivative curve (Table 2).

Table 2.
Characteristic points obtained from thermal-derivative analysis

Point	Temperature	Description
1	T_N	Nucleation of α-phase (liquidus temperature)
2	T_G	The α-Mg dendrite growth temperature
3	$T_{(Mg+Si)}$	Nucleation of Mg_2Si phases
4	$T_{(Mg+Zn)}$	Nucleation of $MgZn_2$ phases
5	T_{sol}	End of solidification (solidus temperature)

2.4. Microstructure examinations

Metallographic samples were taken from a location close to the thermocouple tip. Samples were cold mounted and grounded on 240, 320, 400, 600 and 1200 grit SiC paper and then polished with 6 µm, 3 µm and 1 µm diamond paste. The polished surfaces were etched with a solution of 2 g oxalic acid, 100 ml water, with fresh alcohol blotted repeatedly onto the surface to prevent residue deposits.

The X-ray qualitative and quantitative microanalysis and the analysis of a surface distribution of cast elements in the examined magnesium cast alloys have been made on the Opton DSM-940 scanning microscope with the Oxford EDS LINK ISIS dispersive radiation spectrometer at the accelerating voltage of 15 kV Phase composition and crystallographic structure were determined by the X-ray diffraction method using the X`Pert device with a copper lamp, with 40 kV voltage. The measurement was performed by angle range of 2θ: 35º-120º.

3. Results and discussions

3.1. Thermal analysis results

The cooling curves recorded for MA MgAl6Zn3 alloy at various cooling rates are shown in Fig. 3. It is seen that formation temperatures of the various phases are changed when the cooling rate is increased. The shift magnitude increases with an increasing cooling rate. This shift changes the characteristic parameters of thermal analysis particularly in the liquidus region.

The cooling rate is proportional to the heat extraction from the sample during solidification. Therefore, at a low cooling rate (0.6ºC/s - red line), the rate of heat extraction from the sample is slow and the slope of the cooling curve is small. So, it creates a wide cooling curve. But, at a high cooling rate (2.4ºC/s - blue line) the rate of heat extraction from the sample is fast, the slope of the cooling curve is steep and it makes a narrow cooling curve.

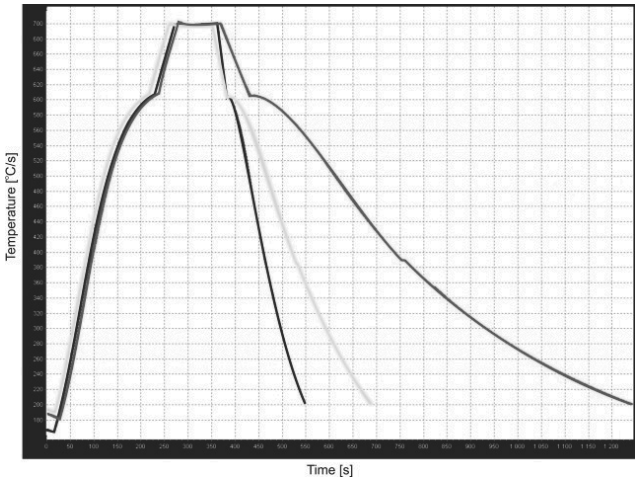

Fig. 3. Cooling curves of MA MgAl6Zn3 alloy at various cooling rates

Thermal analysis of the magnesium alloys have been presented on Figure 4. More detailed information pertaining to the alloy's thermal characteristics such as non-equilibrium liquidus, etc. were determined using the first derivative curves. The most important temperatures of the metallurgical reactions are presented in Table 3. Based on the cooling curve analysis, the non-equilibrium liquidus temperature of MA MgAl6Zn3 alloy that solidified at 0.6°C/s was found approximately 623.0.2±0.82°C. At this temperature the first magnesium dendrites, most likely, nucleated from the melt. Latent heat evolved and caused the temperature of the surrounding melt to rise. This point was clearly visible as a sudden change in the first

derivative curve. The next point corresponded to α-Mg dendrite growth temperature was observed at 605.22±1.17°C. Next important temperatures noted from crystallization curves are nucleation of Mg_2Si and $MgZn_2$ phases. They are respectively 497.03±2.28°C and 392.61±1.09°C. It was found that non-equilibrium solidus temperature was approximately 351.86±1.17°C. Parameters for magnesium alloys that solidify at highest solidification rate are presents in Table 3.

Table 3.
Non-equilibrium thermal characteristics of the MA MgAl6Zn3 alloy test samples obtained during the solidification process at 0.6°C/s, 1.2°C/s and 2.4°C/s solidification rates

Characteristic point	Solidification rate [°C/s]		
	0.6	1.2	2.4
	Temp. [°C]	Temp. [°C]	Temp. [°C]
1	623.0.2±0.82	616.64±12.85	615.04±2.25
2	605.22±1.17	603±0.09	602.98±0.29
3	497.03±2.28	465.56±20.28	494.91±0.62
4	392.61±1.09	388.43±2.04	392.92±1.35
5	351.86±1.17	345.63±1.4	340.04±0.9

Figure 5 shows the variation of the magnesium nucleation temperature as a function of cooling rate. Standard errors calculated for each measured data point have also been included in the graph. It is evidence from the plot, that the Mg nucleation temperature decrease with increase cooling rate from 0.6 to 2.4ºC/s, the Mg nucleation temperature increases from 623.0.2±0.82 to 615.04±2.25°C. Increasing the cooling rate decreases the heat extraction.

Figure 6 presents an influence of cooling rate on the α-Mg dendrite growth temperature. This temperature slightly decreases from 605.22±1.17 to 602.98±0.29°C during increasing cooling rate. Figures 7 and 8 represent an influence of cooling rate on nucleation temperatures of Mg_2Si and $MgZn_2$. Those temperatures are slightly shifting with changing a cooling rate.

Figure 9 presents an influence of cooling rate on solidus temperature. As can be seen that the cooling rate increases cause solidus temperature decreases.

3.2. Structure characteristic

According to the X-ray phase analysis, the investigated MA MgAl6Zn3 alloy cooled with solidification rate: 0.6, 1.2 and 2.4. ºC/s is composed of one phase (Fig. 10): α-Mg solid solution as matrix. In the diffraction pattern of the matrix, the {101} Mg-diffraction line has very intensity. Based on the X-ray phase analysis was found, that change of solidification rate don't influence on the phases composition of investigated alloy.

a)

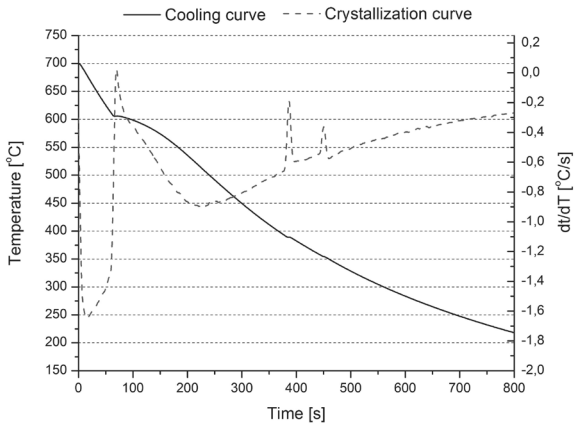

b)

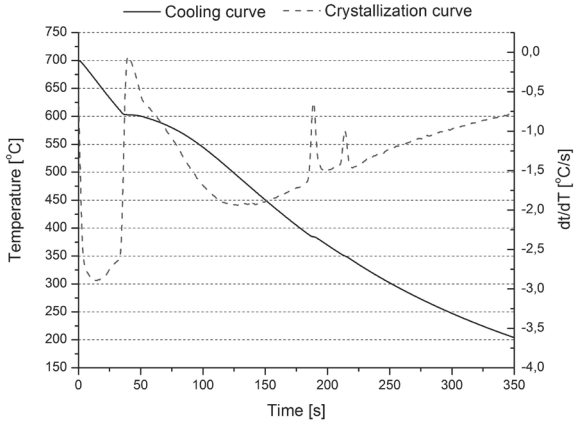

c)

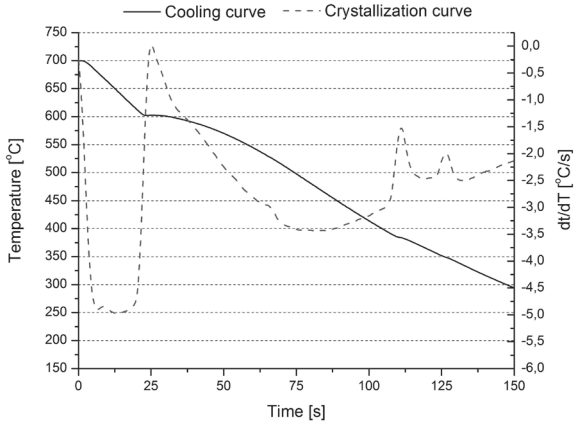

Fig. 4. Cooling, crystallization and calorimetric curves of the magnesium alloy solidified with cooling rate: a) 0.6°C/s, b) 1.2°C/s, c) 2.4°C/s

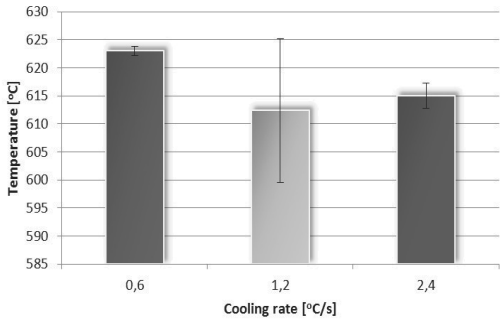

Fig. 5. Variation of the Mg nucleate temperature as a function of cooling rate

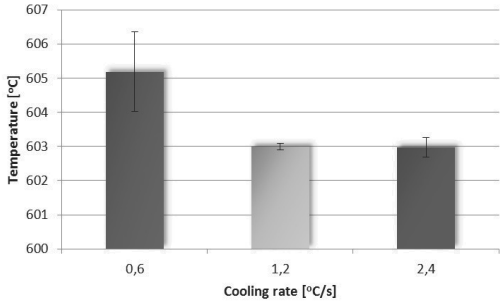

Fig. 6. Variation of the α-Mg dendrite growth temperature as a function of cooling rate

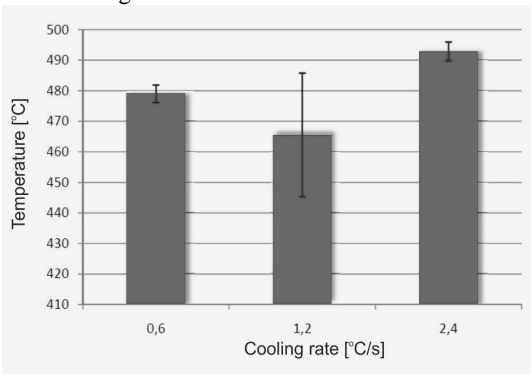

Fig. 7. Variation of the Mg_2Si phase nucleation as a function of cooling rate

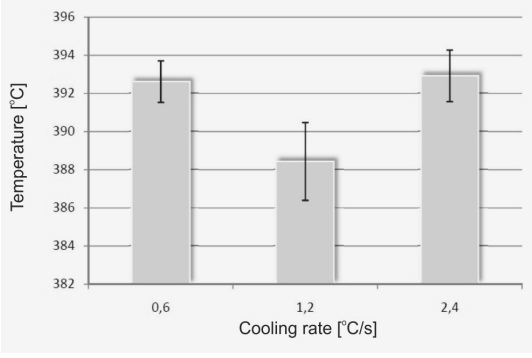

Fig. 8. Variation of the $MgZn_2$ phase nucleation as a function of cooling rate

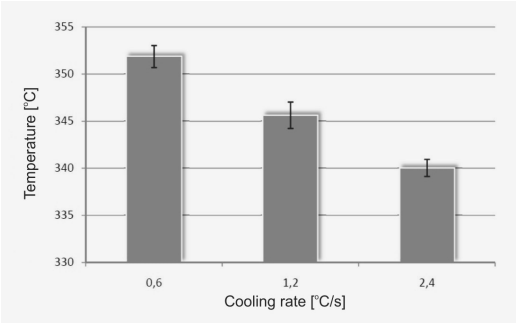

Fig. 9. Variation of the solidus temperature as a function of cooling rate

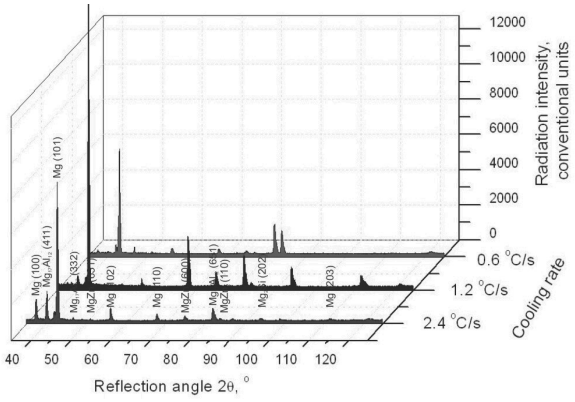

Fig. 10. XRD pattern of MA MgAl6Zn3 casting alloy at various solidification conditions

SEM micrographs of MA MgAl6Zn3 cast after thermal analysis are shown in Figs. 11 and 12. Results from EDS analysis are shown in Table 4. EDS spectra for all samples confirms that, the matrix is α-Mg, and intermetallics phases mostly likely Mg_2Si, and $MgZn_2$. Because the size of particular elements of the structure is, in a prevailing measure, smaller than the diameter of the analyzing beam, the obtained at the quantitative analysis chemical composition may be averaged as a result of which some values of element concentrations may be overestimated.

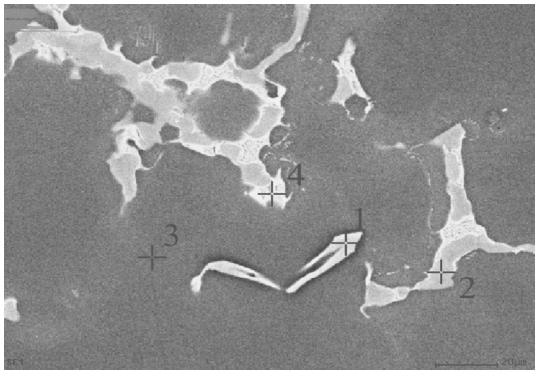

Fig. 11. Representative scanning electron microscope micrograph of magnesium alloy that solidified with cooling rate 0.6°C/s

a)

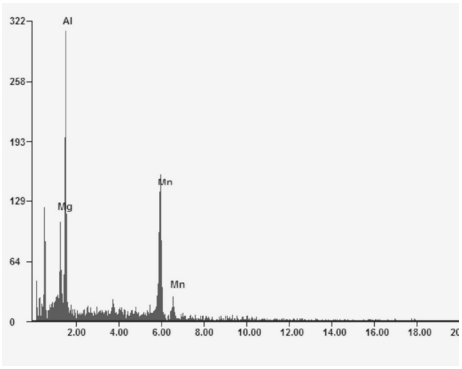

b)

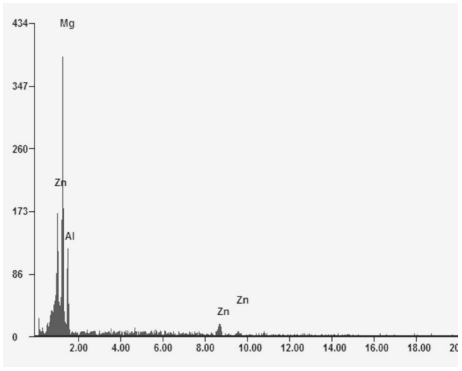

c)

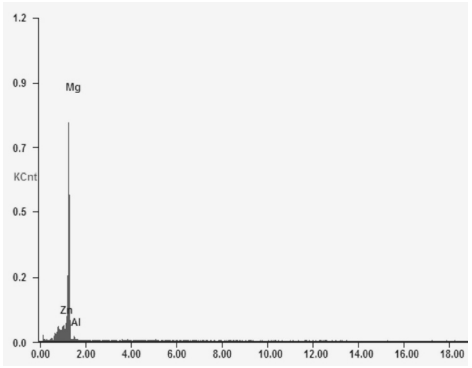

d)

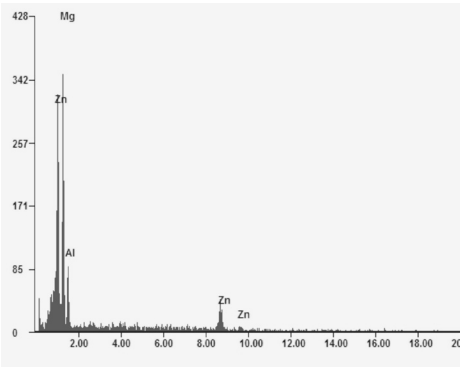

Fig. 12. Spectrum of the pointwise chemical composition analysis: a) point 1, b) point 2, c) point 3, from Fig. 11

Figure 13 shows the solidification microstructures of MA Mg6Zn3 alloys at different cooling rates, which consisted of α-Mg solid solution and $Mg_{17}Al_{12}$, $MgZn_2$ and Mg_2Si compounds located in grain edge. The structure configurations at different experimental cooling rates were similar. The cooling rate had obvious effect on grain size of solidification microstructure. The grain size of magnesium alloy was determined by image analysis, shows that the grain size decreases with increasing cooling rate.

a)

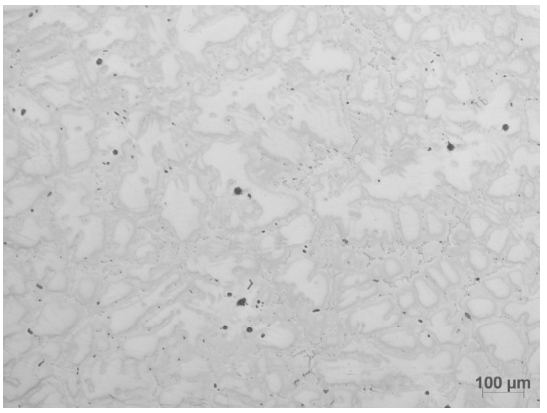

b)

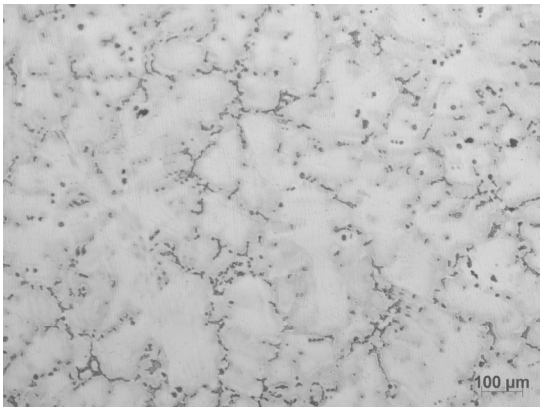

c)

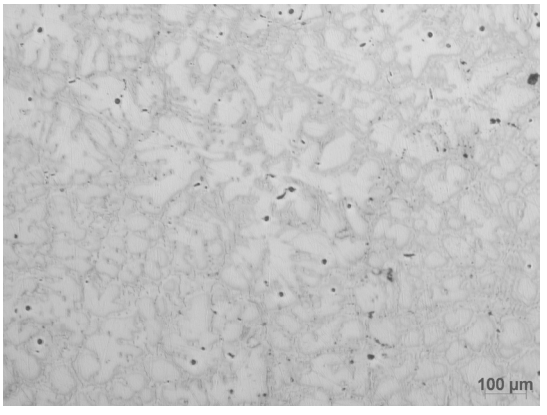

Fig. 13. Microstructures of MA MgAl6Zn3 alloy solidified with cooling rate: a) 0.6°C/s, b) 1.2°C/s, c) 2.4°C/s. Magnification 100x

Table 4.
Pointwise chemical composition analysis from Fig. 11

Analysis	Element	The mass concentration of main elements, %	
		weight	atomic
1	Mg	12.87	19.11
	Al	34.66	46.39
	Mn	52.48	34.5
2	Mg	53.87	63.46
	Al	26.21	27.82
	Zn	19.93	8.73
3	Zn	10.37	4.14
	Mg	86.47	92.81
	Al	3.16	3.06
4	Mg	52.24	67.18
	Al	14.65	16.98
	Zn	33.11	15.84

The grain size decreases from 530 to 380 μm with an increase of CR from 0.6 to 2.4°C/s (Fig. 14).

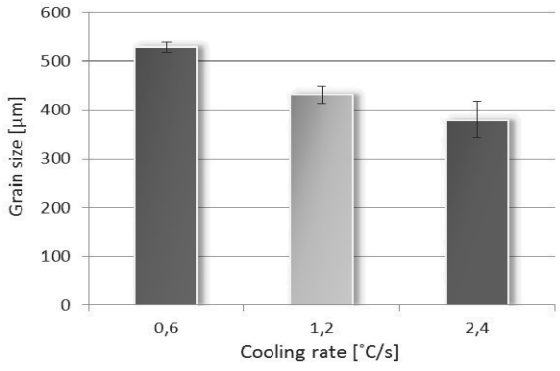

Fig. 14. Effect of cooling rate on grain size analysed magnesium alloy

4. Conclusions

The results are summarized as follows:

1. Solidification parameters are affected by the cooling rate. The formation temperatures of T_N and T_{sol} are changed with an increasing cooling rate.
2. As expected, the results show that grain size reduces as the cooling rate increases.
3. Increasing the cooling rate increases significantly the Mg nucleate temperature, nucleation undercooling temperature and solidification range. These phenomena lead to an increased number of nucleus that affect the size of the grains.
4. The X-ray phase analysis don't ravel occurring of Mg_2Si and phases contains Mn and Al, what suggested that the fraction volume of these phases is below 3%.
5. Increasing the cooling rate increases the ultimate compressive strength.

References

[1] H. Huang, Casting Handbook, Non-ferrous alloy, Mechanical Industry Press, Beijing, 1993.

[2] L.A. Dobrzański, M. Król, T. Tański, Effect of cooling rate and aluminum contents on the Mg-Al-Zn alloys' structure and mechanical properties, Journal of Achievements in Materials and Manufacturing Engineering 43/2 (2010) 613-633.

[3] L. Cížek, R. Korený, I. Juricka, J. Maisner, M. Greger, S. Lasek, P. Betáková, A. Hernas, Structure and properties of the selected magnesium alloys, Proceedings of the 10th Jubilee International Scientific Conference "Achievements in Mechanical and Materials Engineering", AMME'2001, Gliwice - Zakopane, 2001, 75-78.

[4] L. Cížek, A. Hanus, M. Sozańska, T. Tański, L. Pawlica, Structure of magnesium alloys with axmixture of silicon and zirkonium, Acta Metallurgica Slovaca (2007) 531-538.

[5] W. Walke, J. Przondziono, E. Hadasik, J. Szala, D. Kuc, Corrosion resistance of AZ31 alloy after plastic working in NaCl solutions, Journal of Achievements in Materials and Manufacturing Engineering 45/2 (2011) 132-140.

[6] M.M. Avedesian, H. Baker, Magnesium and magnesium alloys, ASM International, Materials Park, USA, 1999.

[7] I.J. Polmear, Light Alloys, Arnold, London, 1995.

[8] C.J. Bettles, D.J. Rossouw, K. Venkatesan: Magnesium alloys and application, Wiley-VCH, New York, 2000.

[9] A. Kiełbus, J. Adamiec, J. Cwajna, J. Paśko, The influence of heat treatment on the microstructure of GA8 magnesium alloy, Journal of Achievements in Materials and Manufacturing Engineering 20 (2007) 131-134.

[10] T. Rzychoń, A. Kiełbus, Microstructure of WE43 casting magnesium alloy, Journal of Achievements in Materials and Manufacturing Engineering 21/1 (2007) 31-34.

[11] T. Rzychoń, A. Kiełbus, G. Dercz, Structural and quantitative analysis of die cast AE44 magnesium alloy, Journal of Achievements in Materials and Manufacturing Engineering 22/2 (2007) 43-46.

[12] D. Kuc, E. Hadasik, G. Niewielski, A. Płachta, Structure and plasticity of the AZ31 magnesium alloy after hot deformation, Journal of Achievements in Materials and Manufacturing Engineering 27/1 (2008) 27-30.

[13] T. Rzychoń, A. Kiełbus, Microstructure and tensile properties of sand cast and die cast AE44 magnesium alloy, Archives of Metallurgy and Materials 50/3 (2008) 901-907.

[14] A. Kiełbus, The influence of casting temperature on castability and structure of AJ62 alloy, Archives of Materials Science and Engineering 28/6 (2007) 345-348.

[15] "Method and Apparatus for Universal Metallurgical Simulation and Analysis" - United States Patent, Patent No.: US 7,354,491 B2, Date of Patent: Apr. 8, 2008.